Research Article

Thabang C. Lebepe, Sundararajan Parani, Rodney Maluleke, Vuyelwa Ncapayi, Olanrewaju A. Aladesuyi, Atsuki Komiya, Tetsuya Kodama, and Oluwatobi S. Oluwafemi*

NIR-II window absorbing graphene oxide-coated gold nanorods and graphene quantum dot-coupled gold nanorods for photothermal cancer therapy

https://doi.org/10.1515/ntrev-2022-0541
received August 13, 2022; accepted March 28, 2023

Abstract: The graphene-based materials have been used as a potential coating material for nanoparticles due to their excellent passivation. Herein, we report for the first time the colloidal stability, photothermal profile, thermal stability, cytotoxicity, and photo-cytotoxicity of graphene quantum dots (GQDs) coupled with the second infrared window (NIR-II) absorbing gold nanorods (AuNRs/GQDs) and compare it to graphene oxide (GO)-coated NIR-II absorbing AuNRs (AuNRs/GO). The composites were achieved by electrostatic interaction of the GO or GQDs with AuNRs. The results revealed that (i) AuNRs/GQDs were more stable in the aqueous phosphate buffer and cell culture media than AuNRs/GO and AuNRs; (ii) GO enhanced the photothermal efficiency of the AuNRs, whereas GQDs reduced it; (iii) GQDs enhanced the photothermal stability of AuNRs than GO; (iv) both AuNRs/GO and AuNRs/GQDs were biocompatible with mouse colon carcinoma (C26) cell lines and malignant fibrous histiocytoma-like, expressing a fusion of the luciferase and enhanced green fluorescent protein genes (KM-Luc/GFP) cell lines; and (v) photo-cytotoxicity of AuNRs/GO and AuNRs/GQDs conducted against C26 cell lines showed significantly improved cell death compared to laser irradiation alone; however, AuNRs/GO exhibited high photo-toxicity than AuNRs/GQDs. This study shows that AuNRs/GO and AuNRs/GQDs composites possess unique properties to improve AuNRs and be utilised in photothermal applications.

Keywords: gold nanorods, graphene oxide, graphene quantum dots, stability, cytotoxicity, photothermal therapy

Abbreviations

AuNRs	gold nanorods
AuNRs/GO	GO-coated AuNRs
AuNRs/GQDs	GQD-coupled AuNRs
C26	mouse colon carcinoma cell lines
CTAB	cetyltrimethylammonium bromide
FTIR	Fourier-transform infrared spectroscopy
GO	graphene oxide
GQDs	graphene quantum dots
KM-Luc/GFP	malignant fibrous histiocytoma-like, expressing a fusion of the luciferase and enhanced green fluorescent protein genes cell lines
LSPR	longitudinal surface plasmon resonance
NIR	near-infrared
NIR-II	second near-infrared window
PTT	photothermal therapy
TEM	transmission electron microscopy
UV-Vis-NIR	ultraviolet-visible-near-infrared

* **Corresponding author: Oluwatobi S. Oluwafemi,** Department of Chemical Science, University of Johannesburg, Johannesburg, 2028, South Africa; Centre for Nanomaterials Sciences Research, University of Johannesburg, Johannesburg, 2028, South Africa, e-mail: oluwafemi.oluwatobi@gmail.com
Thabang C. Lebepe, Sundararajan Parani, Rodney Maluleke, Vuyelwa Ncapayi, Olanrewaju A. Aladesuyi: Department of Chemical Science, University of Johannesburg, Johannesburg, 2028, South Africa; Centre for Nanomaterials Sciences Research, University of Johannesburg, Johannesburg, 2028, South Africa
Atsuki Komiya: Graduate School of Engineering, Institute of Fluid Science, Tohoku University, Sendai, 980-8577, Japan
Tetsuya Kodama: Laboratory of Biomedical Engineering for Cancer, Graduate School of Biomedical Engineering, Tohoku University, Sendai, 980-8575, Japan; Biomedical Engineering Cancer Research Centre, Graduate School of Biomedical Engineering, Tohoku University, Sendai, 980-8575, Japan

1 Introduction

The ability to easily tune gold nanorods' (AuNRs) longitudinal surface plasmon resonance (LSPR) band to absorb and scatter in the near-infrared (NIR) biological window is one of the unique properties that make them essential in photothermal therapy (PTT) over the past two decades [1–3]. Studies have revealed that wavelength in the NIR-II region is ideal for tumour ablation [4] due to its deeper penetration [5]. Cetyltrimethylammonium bromide (CTAB) is a common surfactant used to synthesise AuNRs, and it is a soft template for shape-direct Au seeds into a rod shape and a capping agent. However, it induces cytotoxicity, a major barrier to biological applications. In addition, long-time irradiation usually leads to the thermal reshaping of AuNRs [6,7]. In addressing this problem, polymer coating has been shown to reduce cytotoxicity [8,9] effectively. However, they are ineffective in preventing the reshaping of AuNRs due to their low thermal stability [7,8].

Graphene-based materials such as graphene oxide (GO) and graphene quantum dots (GQDs) are biocompatible materials that are easy to synthesise with cost-effectiveness and scalability. Both GO and GQDs contain a variety of oxygen-bearing functional groups like epoxy, hydroxyl, carbonyl, and carboxylic groups and can be easily functionalised with biomolecules [9,10]. GO, a two-dimensional sheet, exhibits properties such as large surface area, tunable thermal conductivity, and solubility in an aqueous medium [6,11]. GQDs, on the other hand, are small in size, between 2 and 20 nm, and possess exceptional tunable photoluminescence (PL) properties, multi-photon excitation properties, and electrochemiluminescence [12,13]. These graphene-based materials have been applied in different biomedical fields, such as diagnostics, drug delivery, PTT, and *in vitro* and *in vivo* bioimaging [12,14–17]. Researchers in recent years have shown that GO coating of nanomaterials improves their properties, such as drug delivery [6,11], biocompatibility, and photothermal stability [6,17]. The coating of AuNRs with graphene-based material is still an ongoing investigation. Currently, the most investigated AuNRs absorbed in the first biological NIR window (NIR-I) range from 750 to 900 [6,12,14,15,18–23], which is not ideal for deeply embedded tumour ablation [5,6,12,14,15,18–23]. The AuNRs absorbing in the NIR-I have been reported to reshape to a spherical shape and possess blue-shifted LSPR due to the irradiation and coating with GO [19]. These challenges make them lose their NIR absorption properties. In this article, we investigated the coating of NIR-II absorbing AuNRs with GO, and its photothermal profiling was studied for the first time. On the other hand, the coating/coupling of AuNRs with GQDs has not yet been explored for biological applications, especially for PTT, although GQDs have been used to coat or couple with other materials for improved photodynamic efficacy [12,24]. Recently, GQDs have been used as photothermal agents; however, the laser power is high, and the laser exposer is also prolonged, which can result in skin damage [4,25,26]. One way of improving this is by combining the GQDs with AuNRs. This will also improve the biocompatibility of the AuNRs.

Herein, we report for the first time the colloidal stability, thermal stability, cytotoxicity, and photothermal profile of GQDs coupled with that of NIR-II absorbing AuNRs (AuNRs/GQDs) and compare it to NIR-II absorbing GO-coated AuNRs (AuNRs/GO). Briefly, AuNRs, GO, and GQDs were synthesised using the binary-surfactant seed-mediated method, modified Hummer's method, and pyrolysing citric acid (CA), respectively. AuNRs were then coated/coupled with these two graphene materials *ex situ*. The effect of GO and GQDs on AuNRs was evaluated by looking at their colloidal stability, photothermal profiling, photostability, and cytotoxicity against two cancer cells (mouse colon carcinoma [C26] and malignant fibrous histiocytoma-like, expressing a fusion of the luciferase and enhanced green fluorescent protein genes [KM-Luc/GFP]), and photo-cytotoxicity against C26 (Scheme 1). This study shows that AuNR/GO and AuNR/GQD composites possess unique properties, which can be utilised for photothermal applications. In addition, the role of GQDs as a coupling agent for AuNRs has been established in biological applications.

2 Experimental section

2.1 Materials

Hydrogen tetra-chloroauric hydrate ($HAuCl_4{\cdot}xH_2O$, 99.9%), sodium borohydride ($NaBH_4$, 99%), silver nitrate ($AgNO_3$, 99%), CTAB (≥99%), ascorbic acid (AA, 99%), sodium oleate (NaOL, ≥99%), phosphate-buffered saline (PBS, Ca^{2+} and Mg^{2+} free), Roswell Park Memorial Institute (RPMI) 1640 medium, hydrochloric acid (HCl, [12.1 M]), CA, sulphuric acid (H_2SO_4), sodium nitrate ($NaNO_3$), potassium permanganate ($KMnO_4$), peroxide (H_2O_2), graphite powder, and sodium hydroxide (NaOH) were purchased from Sigma-Aldrich, South Africa. All of the gold salt, $AgNO_3$, and $NaBH_4$ solutions were freshly prepared. All glassware used in the experiments were cleaned, washed

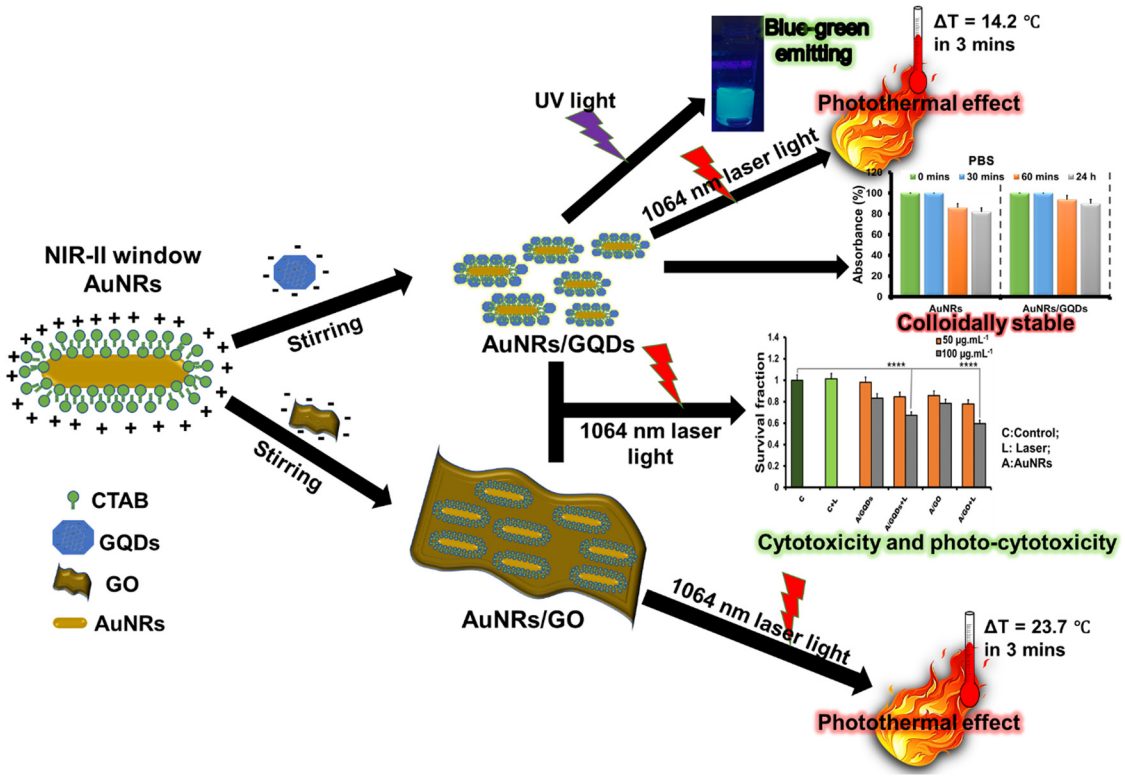

Scheme 1: Schematic illustration of AuNRs coating with GO and coupling with GQDs via electrostatic interaction and characterisation.

thoroughly with MilliQ water (18.0 MΩ cm @ 25°C), and dried before use.

2.2 Synthesis of GO and GQDs

GO was prepared using a modified Hummers method [27]. Briefly, graphite flakes (3 g) and $NaNO_3$ (1.5 g) were added to an ice-cold concentrated H_2SO_4 (69 mL), followed by slow addition of $KMnO_4$ (~10 g) while stirring in an ice bath. The reaction mixture was then warmed to 35°C and stirred for another 30 min before adding MilliQ water (138 mL) in portions. The temperature was further increased to 95°C for 30 min. The obtained deep brown colour solution was cooled to room temperature, and then H_2O_2 (30 mL) was added while stirring. The reaction mixture was left overnight to settle. The product was washed several times with distilled water to neutralise the pH and dried at room temperature to obtain graphite oxide powder. Totally, 50 mg of the graphite oxide was suspended in MilliQ water (50 mL) and ultrasonicated for 2 h to exfoliate as GO sheets. This was followed by centrifugation at 10,000 rpm for 1 h, and the resulting pellet was resuspended in MilliQ water (50 mL) to obtain homogeneous GO dispersion (1.0 mg mL^{-1}).

The GQDs were prepared by direct pyrolysis of CA following the Dong *et al.* method [28]. Briefly, CA (2 g) was placed in a beaker and heated to 200°C using a hotplate for 30 min. The resultant sticky brownish paste was neutralised with 1 L NaOH (10 mg mL^{-1}) solution to produce a GQD solution.

2.3 AuNR synthesis

AuNRs absorbing in the NIR-II window were prepared using a seed-mediated binary-surfactant method according to the previously reported method [2] with some modifications. Briefly, a seed solution was prepared by adding 3.7 g of CTAB powder into 10 mL of warm MilliQ water (40°C) and magnetically stirred until the powder dissolved completely. The solution was then allowed to cool to room temperature, followed by the slow addition of 0.5 mL of $HAuCl_4$ (0.01 M) and gentle stirring for 30 min before adding freshly prepared 0.6 mL of ice-cold 0.01 M $NaBH_4$. The resultant light brown solution was vigorously stirred for 2 min and kept at room temperature for about 30 min. This serves as the gold seed solution.

The surfactant mixture solution was prepared for the growth solution by adding 0.7 g of CTAB and 0.12 g of

NaOL in 25 mL of warm MilliQ water (40°C). This was followed by gentle stirring until it was completely dissolved. Then, 2.4 mL of freshly prepared $AgNO_3$ (4 mM) was added to the surfactant solution and left undisturbed for 15 min, after which 25 mL of $HAuCl_4$ (1 mM) was added. The resulting mixture was stirred for 60 min, and 0.96 mL of HCl (12.1 M) was added, followed by 125 µL of AA (0.064 M), and the solution was stirred vigorously for 1 min. The rod growth process was initiated by adding 4 µL of the seed solution to the growth solution, and the whole solution was stirred for 0.5 min and left undisturbed at 30°C overnight. The AuNRs obtained in the solution were centrifuged at 7,000 rpm for 15 min three times to remove unreacted CTAB and other Au nanoparticles (the suspension was separated from the sediment [reddish and whitish liquid] for each case). The final suspension was centrifuged at 14,000 rpm to concentrate the AuNRs. The precipitated AuNRs were resuspended in MilliQ water.

2.4 GO-coated AuNRs and GQD-coupled AuNRs

The AuNRs/GO was prepared by adding 0.5 mL of AuNRs (optical density [OD]: 1.7 ± 0.034 @ 1,055 nm) into 10 mL of GO (0.05 mg mL^{-1}) solution. The solution was stirred for 30 min, the dispersion solution was centrifuged at 5,000 rpm for 10 min, and the AuNRs/GO suspension was collected for further analysis. AuNRs/GQDs were prepared by following Vinoth *et al.*'s method with slight modifications [29]. Briefly, 0.5 mL of AuNRs (OD: 1.7 ± 0.034 @ 1,055 nm) was added into 10 mL of GQDs (OD: 0.2 ± 0.030 @ 360 nm) solution. After stirring for 30 min, the dispersion solution was centrifuged at 10,000 rpm for 30 min, and the obtained AuNR/GQD pellet was redispersed in 5 mL of MilliQ water for further analysis.

2.5 Characterisation techniques

The ultraviolet-visible-near-infrared (UV-Vis-NIR) absorption spectra of the samples were obtained using a UV-Vis-NIR JASCO V-770 spectrophotometer (JASCO Corp., Japan). The surface chemistry was investigated using spectrum's two UATR spectrometers (Perkin Elmer). X-ray diffraction patterns of the samples were recorded on the Bruker D8 Advance diffractometer. The as-synthesised samples' morphology was captured by high-resolution transmission electron microscopy (JEOL 2010, 200 kV, Japan). The particle size of the AuNRs and composites was measured from TEM images using ImageJ software. Zeta sizer (ELSZ-2000, Japan) was used to measure the surface charge of the samples. The fluorescence spectra of the samples were measured using a spectrofluorophotometer (RF-6000, Japan). For NIR irradiation, a continuous Nd:YV04 air-cooled laser (1,064 nm) with an optical fibre to deliver an 8 mm beam diameter was used.

2.6 Culture medium stability

The stability of AuNRs, AuNRs/GO, or AuNRs/GQDs was tested in two culture media (RPMI and PBS). Briefly, 200 µL of AuNRs, AuNRs/GO, and AuNRs/GQDs was added separately into 2 mL of RPMI (supplemented with 10% fetal bovine serum [FBS], 1% L-glutamine penicillin–streptomycin [L-Glu], and 0.5 % Geneticin G418) in a UV-Vis-NIR quartz cell. The absorbance at 1,055 nm was measured immediately at 30 min, 60 min, and 24 h for all the samples. The same procedure was followed for the stability in PBS (Ca^{2+} and Mg^{2+} free). The media without samples was used as the reference. The absorbance percentage was calculated using the following equation

$$\% A = \frac{A_t}{A_0} \times 100, \quad (1)$$

where % A is the percentage absorbance changes with time, A_t is the absorbance reading at a given time, and A_0 is the initial absorbance reading.

2.7 Photothermal profiling

The photothermal efficiency of AuNRs was measured by placing 1 mL of different concentrations (5–100 µg mL^{-1}) of AuNRs in a 1.5 mL Eppendorf tube, which was irradiated using a 1,064 nm laser at different power densities (0.1, 0.2, 0.25 W cm^{-2}) for 3 min. For comparison, 50 µg mL^{-1} of AuNRs, AuNRs/GO, or AuNRs/GQDs was irradiated using a 1,064 nm laser with a power density of 0.2 W cm^{-2} for 3 min. For photothermal efficiency, reproducibility, and photostability studies, 1 mL of AuNRs, AuNRs/GO, or AuNRs/GQDs (all samples at 100 µg mL^{-1}) were irradiated in a 1.5 mL Eppendorf tube in an ON and OFF cycle with a time interval of 6 min for a period of 1 h using a 1,064 nm laser at a power density of 0.2 W cm^{-2}. The photothermal stability of all the samples after 1 h of irradiation was measured using UV-Vis-NIR spectroscopy.

The temperature changes with time in all experiments were measured using a thermocouple and a thermal camera (FLIRE4 thermal camera). The photothermal conversion efficiency (η) of AuNRs, AuNRs/GO, or AuNRs/GQDs was calculated using equation (2) adapted from Li *et al.'s* with modifications [30].

$$\eta = \frac{hS(T_{max} - T_{surr}) - Q_{Dis}}{I(1 - 10^{-A_{1064}})}, \quad (2)$$

where h is the heat transfer coefficient, S is the surface area of the container, T_{max} is the equilibrium temperature, and T_{surr} is the ambient temperature of the surroundings. Q_{Dis} expresses the heat associated with the light absorbance of H_2O. I is the incident laser power (0.2 W cm^{-2}), and A_{1064} is the absorbance of the sample at 1,064 nm.

2.8 Thermal stability

The thermal stability of AuNRs, AuNRs/GO, or AuNRs/GQDs was determined by incubating 2 mL of AuNRs, AuNRs/GO, and AuNRs/GQDs in separate vials at 50, 60, and 70°C. The changes in absorbance were monitored using UV-Vis-NIR spectroscopy.

2.9 Cell culture, cytotoxicity, and photo-cytotoxicity assays

The cells, mouse colon carcinoma (C26), and malignant fibrous histiocytoma-like, expressing a fusion of the luciferase and enhanced green fluorescent protein genes (KM-Luc/GFP), donated by Tohoku University were cultured in RPMI 1640 (supplemented with 10% FBS and 1% L-Glu) and D-MEM (supplemented with 10% FBS, 0.5% Geneticin G418, and 1% L-Glu), respectively. The cells were then incubated at 37°C in a mixture of 5% carbon dioxide and 95% air until 80% confluence was achieved. The cytotoxicity assay was evaluated by following the standard MTT assay protocol. Briefly, 2 mL of C26 or KM-Luc/GFP cell suspension of the same concentrations (1.0×10^4 cells mL^{-1}) was added to the 12-well plate and incubated at the same condition as the cell culture for 24 h. After 24 h of incubation, cells were exposed to 100 µL of GO, GQDs, AuNRs, AuNRs/GO, or AuNRs/GQDs at different concentrations (5–100 µg mL^{-1}) in triplicate and further incubated for another 24 h. Control cells were not exposed to any samples. After 24 h, 0.2 mL of 3-(4,5-dimethylthiazol-2-yl)-2,5-diphenyltetrazolium bromide (MTT) (5 mg mL^{-1}) solution was added to the cells and incubated at the same condition for 1 h. After that the medium was removed, and 2 mL of dimethyl sulphoxide was added. Totally, 0.1 mL from each well was transferred to a 96-well plate, and the absorbance was measured at a wavelength of 590 nm. For the photo-cytotoxicity assay, the same procedure as above was carried out with AuNRs/GO and AuNRs/GQDs (10, 50, and 100 µg mL^{-1}) followed by irradiation using the 1,064 nm laser for 3 min before cell incubation. The control cells were irradiated without the samples. The blank experiment was carried out without any cells and samples. The survival fraction for both cytotoxicity and photo-cytotoxicity assays was calculated by using the following equation:

$$\text{Survival fraction} = \frac{A_s - A_b}{A_c - A_b}, \quad (3)$$

where A_s is the absorbance of cells with the sample, A_b is the absorbance of the blank sample, while A_c is the absorbance of the cell without the sample, which serves as the control.

2.10 Statistical analysis

Data are presented as mean ± standard error of the mean (SEM). Statistical comparisons were made using Tukey's multiple comparisons tests. Statistically, values of $p < 0.05$ were significant.

3 Results and discussion

3.1 Synthesis and characterisation

GO and GQDs were synthesised using Hummer's method and pyrolysis of CA, respectively. The UV–Vis spectrum of both GO (Figure 1a) and GQDs (Figure 1b) exhibited peaks related to π–π* and n–π* transitions, a characteristic of oxidised graphene-based materials [31]. Figure 1a shows the image of the transmission electron microscopy (TEM) of the GO sheet with clear edges and dark centred due to the folding of the sheets over each other. The TEM image of GQDs (Figure 1b, inset) shows GQDs' particles with an average particle diameter of 2.9 nm. The PL spectra (Figure 1c) show that both GO and GQDs emitted a broad peak at 460 nm. The higher emission intensity of GQDs compared to GO is attributed to their quantum confinement effect [32]. The UV-Vis-NIR spectrum of AuNRs (Figure 1d) shows two peaks, the transversal surface

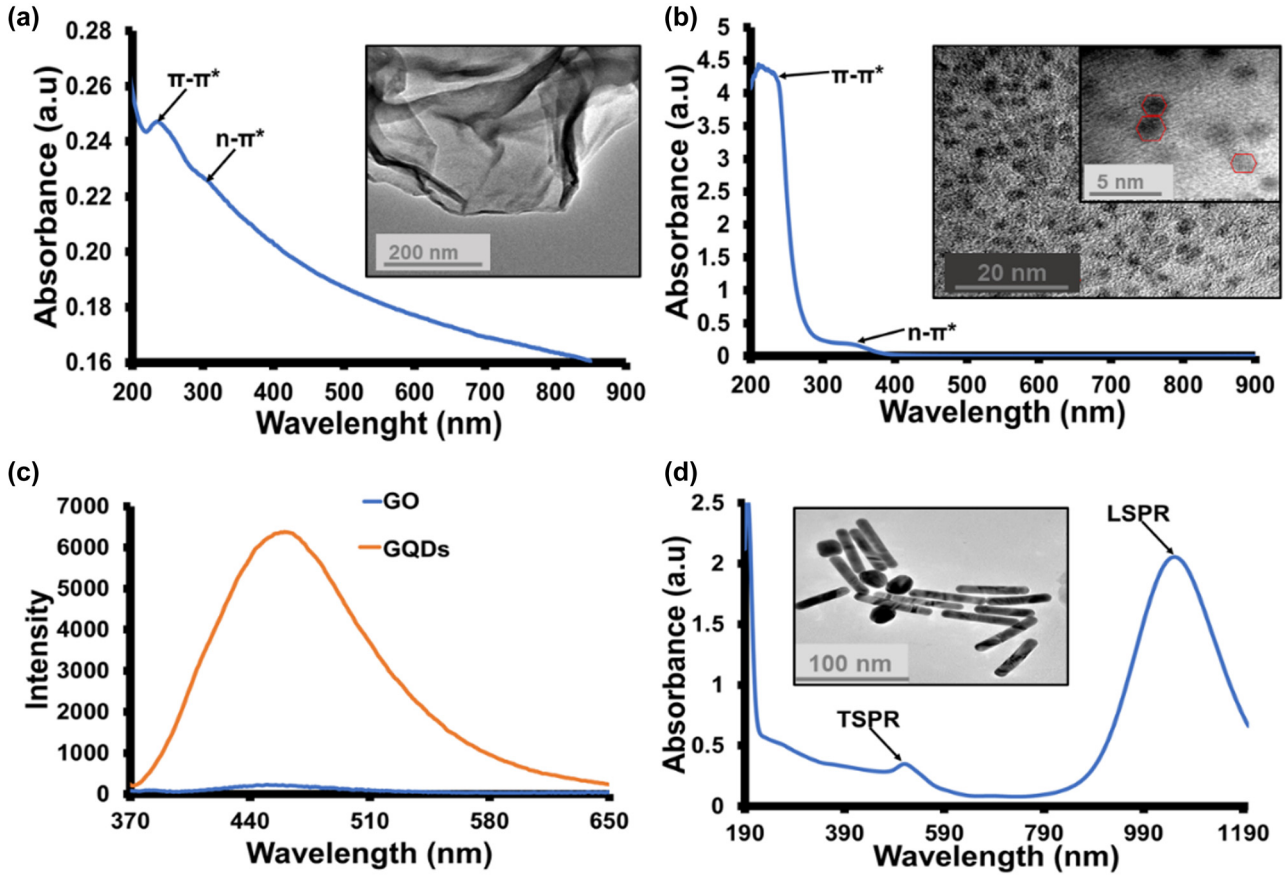

Figure 1: (a) Absorption spectrum of GO, inset: TEM image of GO. (b) The absorption spectrum of GQDs inset: TEM image of GQDs. (c) PL spectra of GO and GQDs (λ_{ex} = 360 nm). (d) The absorption spectrum of AuNRs inset: TEM image of AuNRs.

plasmon resonance at 512 nm and LSPR at 1,055 nm. The TEM image (Figure 1d, inset) shows uniform AuNRs with an average length of 93.2 nm, a width of 6.4 nm (aspect ratio of 14.56), and a few spherical particles with an average diameter of 15 nm. The large-scale TEM image of AuNRs is shown in Figure S1, indicating that the spherical shapes were less in the AuNR sample.

The composites were obtained by coating or coupling AuNRs with GO or GQDs via electrostatic interaction, as illustrated in Scheme 1. The UV-Vis-NIR spectra in Figure 2a and b show that the LSPR peak intensity of AuNRs slightly decreased after the formation of AuNRs/GO and AuNRs/GQDs due to the presence of GO and GQDs. The PL spectrum of AuNRs/GQDs (Figure S2a) shows that it has PL properties similar to GQDs with an emission peak at 460 nm. However, the PL intensity gets reduced, which might be due to the charge transfer from GQDs to AuNRs. In addition, both GQDs and AuNRs/GQDs showed a blue-green emission under UV light (Figure S2b) [28].

The Fourier-transform infrared (FTIR) spectra of the samples are shown in Figure 2c and d. The spectrum of CTAB shows its characteristic peaks, such as long aliphatic methylene C–H asymmetric and symmetric stretching vibrations at 2,916 and 2,849 cm^{-1}, respectively, corresponding C–H bending vibrations with the splitting at 1,473 and 1,463 cm^{-1}, C–H of (CH_3–N^+) asymmetric and symmetric bending vibrations at 1,487 and 1,431 cm^{-1}, respectively, and C–N stretching vibration at 912 cm^{-1}. These vibrations also appeared in the spectrum of AuNRs, however, with the reduced transmittance, suggesting that AuNRs were capped with CTAB molecules. The spectrum of GO shows peaks due to O–H stretching at 3,416 cm^{-1}, C=O vibration shoulder peak at 1,761 cm^{-1}, aromatic C=C stretching at 1,654 cm^{-1}, epoxy and carboxyl vibrations between 1,230 and 1,320 cm^{-1}, which is also seen in the spectrum of GQDs [23,33,34]. The spectrum of both AuNRs/GO and AuNRs/GQDs exhibited peaks attributed to both CTAB-capped AuNRs and the GO or GQDs, indicating the successful formation of the composites [28]. The XRD spectrum of AuNRs/GO shows a strong graphene-like broad peak at 24.8°, which corresponds to the crystalline plane (002), and a small AuNRs peak at 38.8° corresponding to

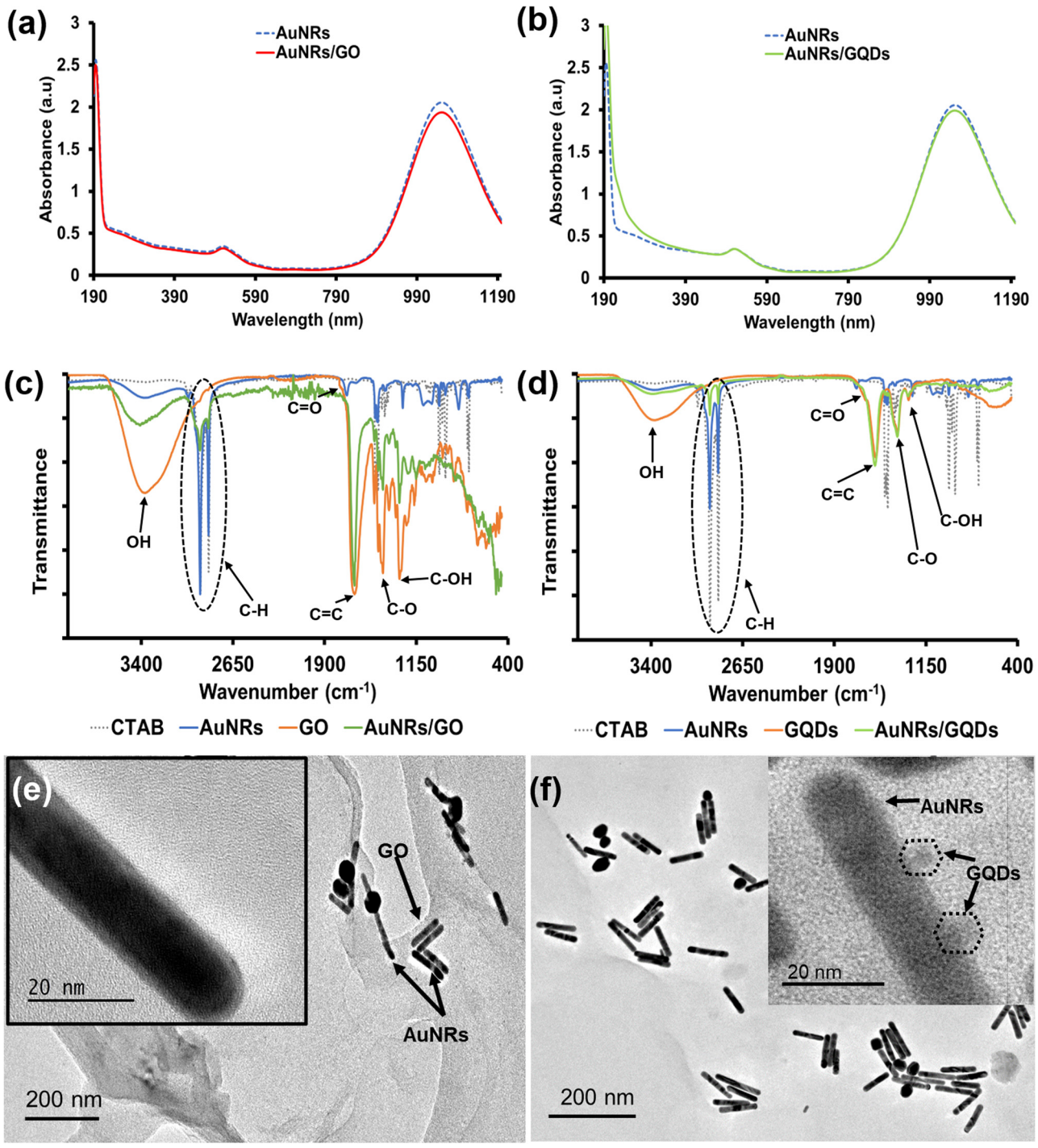

Figure 2: Absorption spectra of (a) AuNRs/GO and (b) AuNRs/GQDs. (c) FTIR spectra of AuNRs, GO, and AuNRs/GO. (d) FTIR spectra of AuNRs, GQDs, and AuNRs/GQDs. (e) TEM image of AuNRs/GO (scale 200 and 20 nm) and (f) TEM image of AuNRs/GQDs (scale 200 and 20 nm).

the (111) plane (Figure S2c) [29]. The XRD pattern of AuNRs/GQDs demonstrated similar peaks as AuNRs/GO with a broad peak at 24.8 associated with graphene structure from the GQDs and a minor peak indexed (100) at ~14° attributed to the interaction of GQDs carbon with the nitride from CTAB [35,36]. In addition, a well-defined diffraction peak at $2\theta = 38.8°$ assigned to the (111) crystalline plane of AuNRs was also present, indicating the presence of both materials in the composite (Figure S2d).

The charge on the surface of AuNRs before and after coating with GO or coupling with GQDs was measured using a zeta potential analyser (Figure S3). The AuNRs

were positively charged due to CTAB on their surface, while the GO and GQDs were negatively charged because of the oxygenated functional groups found in both materials. The positive charge on AuNRs decreased when negatively charged GO and GQDs were introduced, which suggested an electrostatic interaction between AuNRs and GO or GQDs [37]. The zeta potential of AuNRs was reduced from 43.30 to 16.50 mV by the GO sheet, while it was reduced to 28.76 mV by GQDs. We believe that though GQDs were highly negatively charged, they did not interact fully with AuNRs. In the AuNRs/GO composites, GO interacted more with AuNRs because GO sheets have a high surface area that can accommodate AuNRs by multiple bonding. The TEM image of AuNRs/GO shows that the AuNRs are located on the surface of the GO sheet (Figure 2e), while the TEM image of AuNRs/GQDs confirms the coupling of GQDs on AuNRs (Figure 2f). The hydrodynamic size distribution also showed the presence of GQDs and GO in the composite with extra peaks (Figure S4).

3.2 Culture medium stability and photothermal profiling

It is important to understand the colloidal stability of all nanomaterials before applying them to any biological application. Accordingly, the colloidal stability of AuNRs, AuNRs/GO, and AuNRs/GQDs was investigated in supplemented RPMI 1640 cell culture medium and phosphate buffer solution (PBS) by measuring the LSPR absorption of AuNRs. PBS was chosen because of its identical osmolarity and ion concentration with human blood and is widely used in biological research. On the other hand, The RPMI was chosen because it is one of the commonly used media for mammalian cell culture, and it is a media we used to culture the C26 cell line. The difference between RPMI and DMEM (medium used for the cell culture) is that the RPMI comprises glutathione and high concentrations of vitamins such as biotin, vitamin B_{12}, and *para*-aminobenzoic acid, which are not found in DMEM [38,39]. The results showed that AuNRs were stable in supplemented

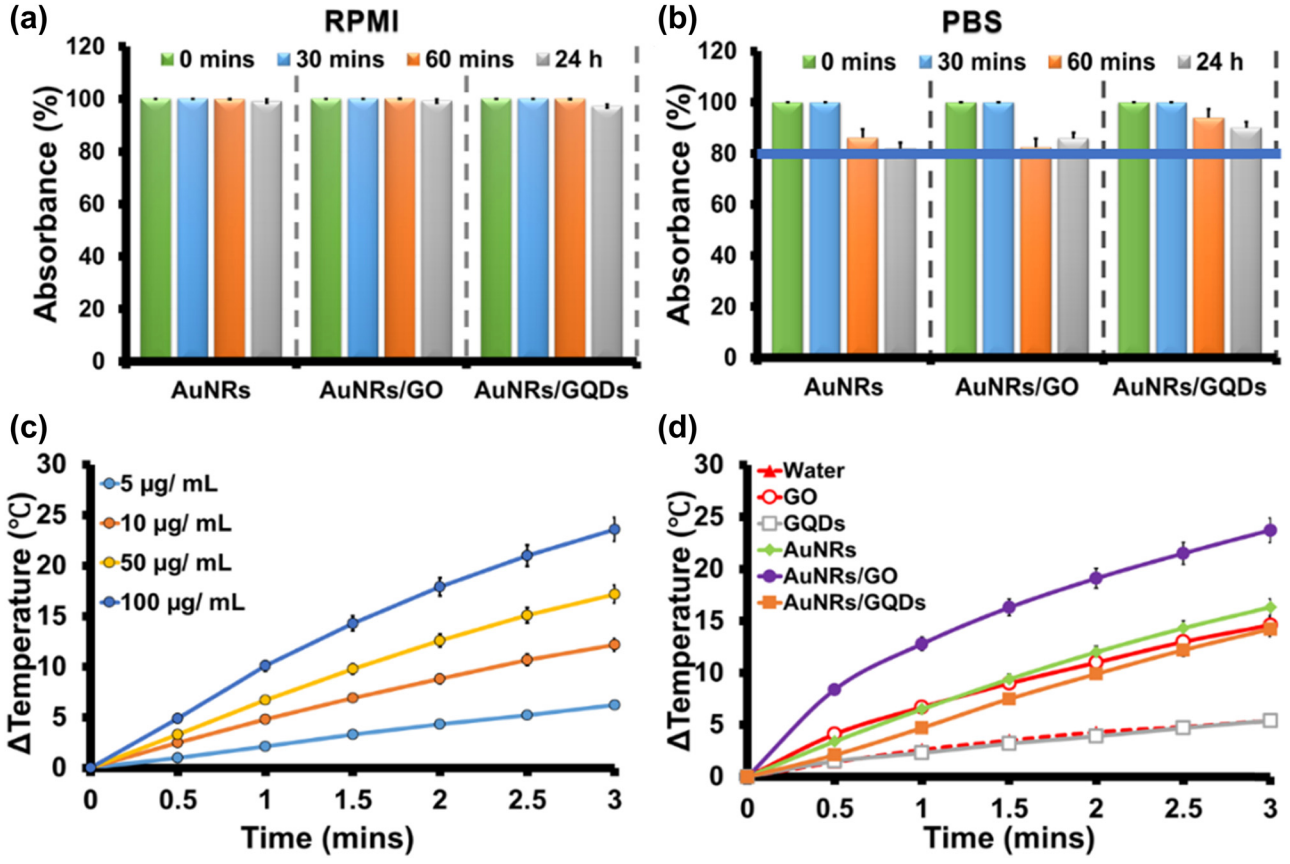

Figure 3: Medium stability of AuNRs, AuNRs/GO, and AuNRs/GQDs nanocomposites in (a) RPMI and (b) PBS at different times. (c) Photothermal response at different concentrations using bare AuNRs after irradiation with laser at 0.2 W cm^{-2} for 3 min. (d) Photothermal response of water, GO, GQDs, AuNRs, AuNRs/GO, and AuNRs/GQDs (50 µg mL^{-1}) with time after irradiation with a laser at 0.2 W cm^{-2} for 3 min.

RPMI for 24 h, and the same effect was also observed with AuNRs/GO and AuNRs/GQDs (Figure 3a). This shows that these graphene materials do not affect the AuNRs' stability in the RPMI medium.

In contrast, when the samples were mixed with the PBS, AuNRs started losing their absorbance intensity significantly after an hour, and the same trend was observed with the AuNRs/GO composite (Figure 3b). The reduction of absorbance might be due to the aggregation of AuNRs caused by the ions found in the PBS solution, and for the AuNRs/GO, it is possible that some of the AuNRs were repelled from the GO surface hence a sight-increasing absorbance after 24 h. However, when GQDs were used, there was an improvement in the stability by 5% when compared to GO after 24 h in PBS. It is worth noting that both composites maintained above 80% stability after 24 h.

Photothermal efficiency was evaluated by irradiating the samples using a 1,064 nm laser. Initially, the deionised water was irradiated with different power densities (0.1, 0.2, and 0.25 W cm^{-2}) as a baseline, and the following changes in temperature (ΔT) were obtained 0.1, 5.4, and 15.8°C with the initial temperature of 29°C, respectively (Figure S5). The power densities in these regions were chosen to be lower than the reported threshold value (0.42 W cm^{-2}), which can lead to skin damage [4]. The initial temperature was set at 29°C for all the samples before irradiation. It has been reported that intracellular temperatures between 40 and 47°C produced during photothermal application can permanently destroy cancer cellular proteins and impair DNA function, which causes apoptotic cancer cell death. On the other hand, temperature above 50°C results in necrosis in cancer cells and rapid cell death in normal cells [26]. The AuNRs (100 μg mL^{-1}) were also irradiated at the same power density for 3 min to evaluate the effect of power density. The ΔT value increased by 1.3, 24.2, and 50.4°C with increased power density (Figure S5). From the results, the laser power density of 0.2 W cm^{-2} was used to optimise the different concentrations of AuNRs that will lead to cell death. Different concentrations of AuNRs (5, 10, 50, and 100 μg mL^{-1}) were irradiated for 3 min (Figure 3c). The ΔT value was found to increase as the concentration increased. At the concentration of 50 μg mL^{-1}, the AuNRs produced a ΔT of 16.3°C. The photothermal efficacy of the composites was evaluated using this concentration and compared to AuNRs. The ΔT values obtained after irradiating AuNRs, GO, GQDs, AuNRs/GO, and AuNRs/GQDs for 3 min were 16.3, 14.6, 5.4, 23.7, and 14.2°C, respectively. The AuNRs/GO demonstrated a higher temperature increase when compared to the AuNRs, GO, GQDs, and AuNRs/GQDs (Figure 3d). The temperature increase can be attributed to enhancing photon absorption of AuNRs/GO when irradiated with a laser [6]. For comparison, water was irradiated for 3 min, and only 5.4°C ΔT was observed. This shows that the majority of the photothermal effects come from the samples. In contrast to AuNRs/GO, the AuNRs/GQDs temperature was lower than that of AuNRs alone. This might be attributed to the ability of GQDs to absorb at longer wavelengths [40,41], which in return reduced the amount of energy available to be absorbed by AuNRs. Photographic images of AuNRs, AuNRs/GO, and AuNRs/GQDs temperature changes were captured using an IR camera (FLIRE4 thermal camera) at 0 and 3 min. The results showed almost similar temperature changes to the digital thermocouple (Figure S6).

Studies have shown that during *in vivo* experiments, prolonged exposure to laser causes skin damage; however, reducing the exposure time through the ON and OFF cycle might reduce the risk of skin damage [4,42–44]. A photothermal ON and OFF cycle was performed at 6 min intervals to investigate the efficiency and stability of AuNRs/GO and AuNRs/GQDs against AuNRs at the same concentration (Figure 4a). The AuNRs/GO composite maintained its heat production throughout the experiment compared to AuNRs and AuNRs/GQDs. On the other hand, AuNRs/GQDs increase their heat production; however, heat loss between the cycles is slow. The effect of prolonged exposure of the as-synthesised materials to laser light was also analysed using UV-Vis-NIR (Figure 4b–d). Figure 4b shows that the AuNRs LSPR peak was blue-shifted (~22.5 nm) from 1,055 to 1032.5 nm with a decrease in absorbance. This could be attributed to the shortening of the AuNR's length [7,8,16]. The absorption spectra of AuNRs/GO (Figure 4c) before and after irradiation show a significant decrease in absorbance, change in spectral shape, and blue-shifted wavelength (~3 nm). The UV-Vis-NIR spectrum of AuNRs/GQDs in Figure 4d shows that it is also blue shifted (13 nm) with a decrease in absorbance; however, this decrease is smaller than the result obtained for AuNRs/GO. These results indicate that though the heat production of AuNRs/GO is constant, it damages the AuNR's length. This behaviour has been reported for GO-coated AuNRs. According to Pan *et al.* [19], the AuNRs on the GO surface tend to reshape as the heat increase to 50°C. This was attributed to the interaction of GO with CTAB on the surface of AuNRs, which becomes stronger as the heat increases. Therefore, causing the CTAB to be stripped off from the surface of AuNRs, thus making the AuNRs unstable, which might also lead to aggregation, hence decreasing the LSPR peak absorbance and wavelength [19]. The thermal stability was done using an incubator at different temperatures (50–70°C) for 30 min. The results showed that all materials were stable at all

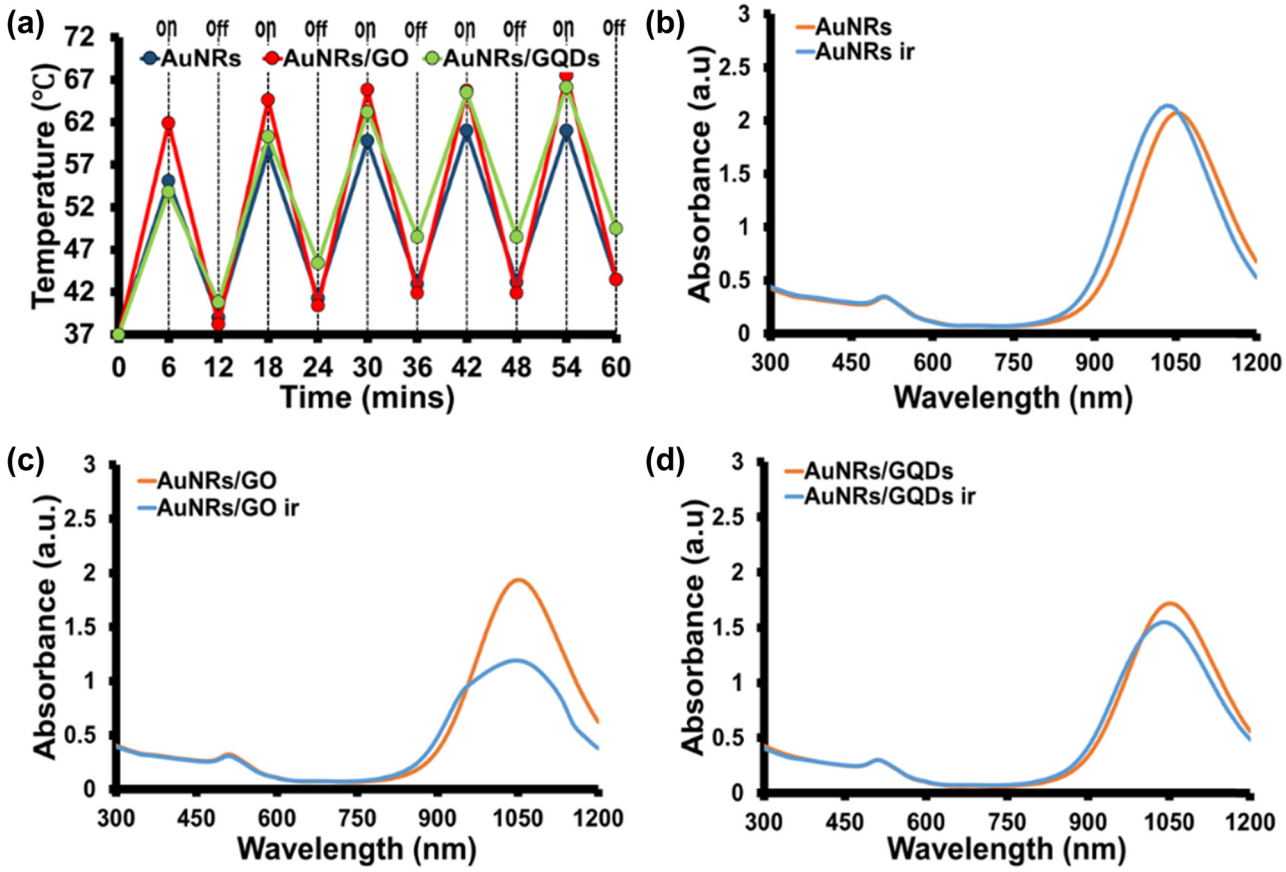

Figure 4: (a) Photothermal efficiency of AuNRs, AuNRs/GO, and AuNRs/GQDs in ON and OFF irradiation cycle at 6 min intervals for 1 h using 1,064 nm laser (0.2 W cm^{-2}). The UV-Vis-NIR spectra of (b) AuNRs, (c) AuNRs/GO, (d) AuNRs/GQDs at a concentration of 100 µg/mL before and after-irradiation in ON and OFF cycle for 1 h with 1,064 nm laser at 0.2 W cm^{-2}.

temperatures, even when the incubation time increased from 30 to 60 min at 70°C (Figure S7). These results show that the external heat effect differs from the internal heat effect. The limitation of AuNRs to absorb the energy when coupled with GQDs is responsible for the AuNRs/GQDs' higher photostability compared to AuNRs and AuNRs/GO, which was interfering with the CTAB–GO bond. The photothermal conversion efficiency of AuNRs, AuNRs/GO, and AuNRs/GQDs was calculated to be 18.75, 15.70, and 13.78%, using equation (2) and data in Figure S8.

3.3 Cytotoxicity and photo-cytotoxicity evaluation

Cytotoxicity of AuNRs, AuNRs/GO, and AuNRs/GQDs was evaluated against two cancer cell lines (C26 and KM-Luc/GFP cell lines) using the MTT assay (Figure 5a and b). The results show that GO and GQDs were biocompatible, with cell viability above 95% in all concentrations. The AuNRs showed toxicity towards both cells in a concentration-dependent trend due to the inherent toxicity of the CTAB capping group [6]. The MTT assay against the C26 cell lines (Figure 5a) shows that coating/coupling of AuNRs with GO or GQDs reduces the toxicity of the bare AuNRs. The cell viability improved by 49% and 46% for AuNRs/GO and AuNRs/GQDs, respectively, at 100 µg mL^{-1}. This improvement also confirmed the uptake of the AuNRs/GO and AuNRs/GQDs by the cell after the coating. However, more analysis is needed to investigate this further. When the composites were tested against KM-Luc/GFP, it was observed that GO improved AuNR biocompatibility by 64%, while GQDs improved it by 80.5% at the highest concentration of 100 µg mL^{-1} (Figure 5b).

The photo-cytotoxicity of AuNRs/GO and AuNRs/GQDs at two concentrations (50 and 100 µg mL^{-1}) was evaluated against C26 cell lines (Figure 5c). The cells irradiated without the sample showed a slight increase in cell viability compared to the control. This could be due to the cellular stress caused by heat from the laser. It has been reported that low-level laser therapy alone leads to proliferation due to the potential modulation of

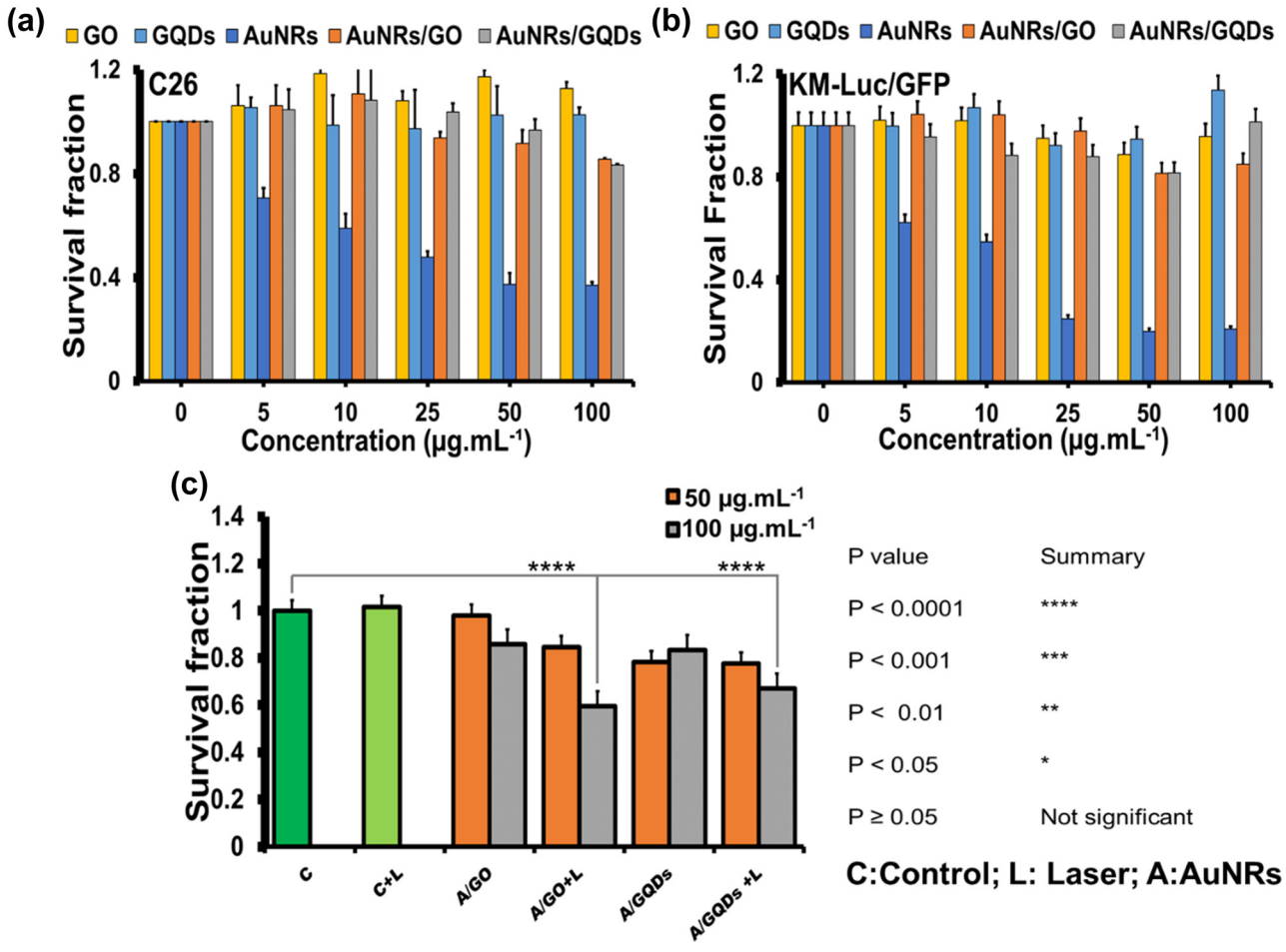

Figure 5: Cell viability of AuNRs (1,066 nm) and graphene-based AuNR nanocomposite against (a) C26 and (b) KM-Luc/GFP cell lines. (c) Photo-cytotoxicity at 50 and 100 μg mL^{-1} of AuNRs/GO and AuNRs/GQDs composite against C26 cell lines at 0.2 W cm^{-2} for 3 min.

angiogenesis in cancer cells by laser [45]. The AuNRs/GO and AuNRs GQDs at 50 μg mL^{-1} showed a partial decrease after irradiation compared to the control. At 100 μg mL^{-1}, highly significant cell abatement of about 19 and 16% was observed for AuNRs/GO and AuNRs/GQDs, respectively. Statistical analysis shows that GO and GQDs effectively improve AuNRs cell abatement upon irradiation. For future studies, we recommend further experiments using a higher concentration for each group or extending the irradiation time to achieve the lowest survival fraction of 50%. From the results, we can confirm that both composites can potentially be used for photothermal tumour ablation.

4 Conclusions

In summary, GO sheets and GQDs were successfully synthesised using Hummer's method and pyrolysis of CA, respectively. The UV–Vis and FTIR spectra confirm the formation of GO and GQDs, while PL spectra showed that GQDs are highly photoluminescent than GO. The AuNRs with an average size of 93.2 nm by 6.4 nm with absorption in NIR-II (1,055 nm) were synthesised using the binary-surfactant seed-mediated method. The AuNRs/GO and AuNRs/GQDs composites were prepared using electrostatic interaction and were confirmed using UV-Vis-NIR, FTIR, and TEM. The effects of coating/coupling AuNRs with GO or GQDs were evaluated based on media stability, photothermal efficiency, cytotoxicity, and photo-cytotoxicity. Both AuNRs/GO and AuNRs/GQDs composites were stable in the culture media RPMI and PBS for 24 h. The photothermal study showed that GO coating improved the photothermal conversion efficiency of AuNRs, while GQDs reduced it. In addition, AuNRs/GQDs exhibited higher photothermal stability than AuNRs/GO. However, the GO high heat production led to significant AuNRs reshaping compared to GQDs. The ON and OFF photothermal efficiency showed that AuNRs/GO and AuNRs/GQDs displayed consistent

heat production. The limitation of AuNRs to absorb the energy when coupled with GQDs is responsible for the AuNRs/GQDs' higher photostability compared to AuNRs and AuNRs/GO, which interfered with the CTAB–GO bond. MTT cell viability assays against C26 and KM-Luc/GFP cell lines showed that both AuNRs/GO and AuNRs/GQDs composites were biocompatible compared to bare AuNRs. The photo-cytotoxicity against C26 cell lines showed that AuNRs/GO is more effective than AuNRs/GQDs. This study demonstrated that these two nanocomposites behaved differently when coated/coupled with AuNRs, with GQDs having better colloidal stability and higher photothermal stability, while AuNRs/GO displayed higher photothermal production at a short period, which gave it an advantage in the photo-cytotoxicity assay. These properties, together with their high media stability and biocompatibility, make these two composites a promising material for theragnostic applications. We believe that GQDs have the potential to be used as a coupling agent for metal nanoparticles in the nanomedicine fields.

Acknowledgments: The authors would like to thank the University of Johannesburg, South Africa, the research committee (URC), and the Faculty of Science Research Committee (FRC) for financial support.

Funding information: This work was supported by National Research Foundation (NRF), South Africa, under South Africa/Japan bilateral program (Grant no: 108669), Equipment-Related Travel and Training grants (Grant no: 118666), Competitive Program for Rated Researchers (Grant nos: 106060 and 129290), and Freestanding Doctoral Scholarship (Grant no: 112867 and 131237).

Author contributions: Conceptualisation: S. O. Oluwafemi; methodology: S. O. Oluwafemi, T. Kodama, A. Komiya; formal analysis and investigation: T. C. Lebepe; writing – original draft preparation: T. C. Lebepe; writing – review and editing: S. Parani, S. O. Oluwafemi; funding acquisition: S. O. Oluwafemi; resources: S. O. Oluwafemi, A. Kodama, T. Komiya; supervision: S. O. Oluwafemi, A. Kodama; data curation and project coordinating: R. Maluleke, V. Ncapayi, O. A. Aladesuyi.

Conflict of interest: The authors declare no conflict of interest.

Data availability statement: The datasets generated during and/or analysed during the current study are available from the corresponding author on reasonable request.

References

[1] Burrows ND, Harvey S, Idesis FA, Murphy CJ. Understanding the seed-mediated growth of gold nanorods through a fractional factorial design of experiments. Langmuir. 2017;33(8):1891–907.
[2] Ye X, Gao Y, Chen J, Reifsnyder DC, Zheng C, Murray CB. Seeded growth of monodisperse gold nanorods using bromide-free surfactant mixtures. Nano Lett. 2013;13(5):2163–71.
[3] Park JE, Kim M, Hwang JH, Nam JM. Golden opportunities: Plasmonic gold nanostructures for biomedical applications based on the second near-infrared window. Small Methods. 2017;1(3):1600032.
[4] Sugiura T, Matsuki D, Okajima J, Komiya A, Mori S, Maruyama S, et al. Photothermal therapy of tumors in lymph nodes using gold nanorods and near-infrared laser light with controlled surface cooling. Nano Res. 2015;8(12):3842–52.
[5] Li X, Zhou J, Dong X, Cheng WY, Duan H, Cheung P. In Vitro and In Vivo photothermal cancer therapeutic effects of gold nanorods modified with mushroom β-glucan. J Agric Food Chem. 2018;66(16):4091–8.
[6] Khan MS, Pandey S, Bhaisare ML, Gedda G, Talib A, Wu HF. Graphene oxide@gold nanorods for chemo-photothermal treatment and controlled release of doxorubicin in mice Tumor. Colloids Surf B: Biointerfaces. 2017;160:543–52.
[7] Horiguchi Y, Honda K, Kato Y, Nakashima N, Niidome Y. Photothermal reshaping of gold nanorods depends on the passivating layers of the nanorod surfaces. Langmuir. 2008;24(20):12026–31.
[8] Zhang Z, Shi J, Song Z, Zhu X, Zhu Y, Cao S. A synergistically enhanced photothermal transition effect from mesoporous silica nanoparticles with gold nanorods wrapped in reduced graphene oxide. J Mater Sci. 2018;53(3):1810–23.
[9] Singh DP, Herrera CE, Singh B, Singh S, Singh RK, Kumar R. Graphene oxide: An efficient material and recent approach for biotechnological and biomedical applications. Mater Sci Eng C. 2018;86:173–97.
[10] McCallion C, Burthem J, Rees-Unwin K, Golovanov A, Pluen A. Graphene in therapeutics delivery: Problems, solutions and future opportunities. Eur J Pharm Biopharm. 2016;104:235–50.
[11] Muazim K, Hussain Z. Graphene oxide—A platform towards theranostics. Mater Sci Eng C. 2017;76:1274–88.
[12] Lebepe TC, Parani S, Oluwafemi OS. Graphene oxide-coated gold nanorods: Synthesis and applications. Nanomaterials. 2020;10(11):2149.
[13] Song D, Guo H, Huang K, Zhang H, Chen J, Wang L, et al. Carboxylated carbon quantum dot-induced binary metal–organic framework nanosheet synthesis to boost the electrocatalytic performance. Mater Today. 2022;54:42–51.
[14] Turcheniuk K, Dumych T, Bilyy R, Turcheniuk V, Bouckaert J, Vovk V, et al. Plasmonic photothermal cancer therapy with gold nanorods/reduced graphene oxide core/shell nanocomposites. RSC Adv. 2016;6(2):1600–10.
[15] Xu C, Yang D, Mei L, Li Q, Zhu H, Wang T. Targeting chemo-photothermal therapy of hepatoma by gold nanorods/graphene oxide core/shell nanocomposites. ACS Appl Mater Interfaces. 2013;5(24):12911–20.
[16] Moon H, Kumar D, Kim H, Sim C, Chang JH, Kim JM, et al. Amplified photoacoustic performance and enhanced

photothermal stability of reduced graphene oxide coated gold nanorods for sensitive photoacoustic imaging. ACS Nano. 2015;9(3):2711–9.
[17] Wei Q, Ni H, Jin X, Yuan J. Graphene oxide wrapped gold nanorods for enhanced photothermal stability. RSC Adv. 2015;5(68):54971–77.
[18] Azerbaijan MH, Bahmani E, Jouybari MH, Hassaniazardaryani A, Goleij P, Akrami M, et al. Electrospun gold nanorods/graphene oxide loaded-core–shell nanofibers for local delivery of paclitaxel against lung cancer during photo-chemotherapy method. Eur J Pharm Sci. 2021;164:105914.
[19] Pan H, Low S, Weerasuriya N, Shon YS. Graphene oxide-promoted reshaping and coarsening of gold nanorods and nanoparticles. ACS Appl Mater Interfaces. 2015;7(5):3406–13.
[20] Qi Z, Shi J, Zhu B, Li J, Cao S. Gold nanorods/graphene oxide nanosheets immobilised by polydopamine for efficient remotely triggered drug delivery. J Mater Sci. 2020;55(29):14530–43.
[21] Qiu X, You X, Chen X, Chen H, Dhinakar A, Liu S, et al. Development of graphene oxide-wrapped gold nanorods as robust nanoplatform for ultrafast near-infrared SERS bioimaging. Int J Nanomed. 2017;12:4349–60.
[22] Sun B, Wu J, Cui S, Zhu H, An W, Fu Q, et al. In situ synthesis of graphene oxide/gold nanorods theranostic hybrids for efficient tumor computed tomography imaging and photothermal therapy. Nano Res. 2017;10(1):37–48.
[23] Tomasella P, Sanfilippo V, Bonaccorso C, Cucci LM, Consiglio G, Nicosia A, et al. Theranostic nanoplatforms of thiolated reduced graphene oxide nanosheets and gold nanoparticles. Appl Sci. 2020;10(16):5529.
[24] Fan H-y, Yu XH, Wang K, Yin YJ, Tang YJ, Tang YL, et al. Graphene quantum dots (GQDs)-based nanomaterials for improving photodynamic therapy in cancer treatment. Eur J Med Chem. 2019;182:111620.
[25] Wang H, Mu Q, Wang K, Revia RA, Yen C, Gu X, et al. Nitrogen and boron dual-doped graphene quantum dots for near-infrared second window imaging and photothermal therapy. Appl Mater Today. 2019;14:108–17.
[26] Khot MI, Andrew H, Svavarsdottir HS, Armstrong G, Quyn AJ, Jayne DG. A review on the scope of photothermal therapy–based nanomedicines in preclinical models of colorectal cancer. Clin Colorectal Cancer. 2019;18(2):e200–9.
[27] Sakho EHM, et al. Dynamic energy transfer in non-covalently functionalised reduced graphene oxide/silver nanoparticle hybrid (NF-RGO/Ag) with NF-RGO as the donor material. J Mater Sci Mater Electron. 2017;28(3):2651–9.
[28] Dong Y, Shao J, Chen C, Li H, Wang R, Chi Y, et al. Blue luminescent graphene quantum dots and graphene oxide prepared by tuning the carbonisation degree of citric acid. Carbon. 2012;50(12):4738–43.
[29] Vinoth V, Rozario TMD, Wu JJ, Anandan S, Ashokkumar M. Graphene quantum dots anchored gold nanorods for electrochemical detection of glutathione. ChemistrySelect. 2017;2(17):4744–52.
[30] Li X, Zhou J, Dong X, Cheng WY, Duan H, Cheung P. In Vitro and In Vivo photothermal cancer therapeutic effects of gold nanorods modified with mushroom β-glucan. J Agric Food Chem. 2018;66(16):4091–8.
[31] Dideikin AT, Vul' AY. Graphene oxide and derivatives: The place in graphene family. Front Phys. 2019;6:149.
[32] Sk MA, Ananthanarayanan A, Huang L, Lim KH, Chen P. Revealing the tunable photoluminescence properties of graphene quantum dots. J Mater Chem C. 2014;2(34):6954–60.
[33] Lebepe TC, Parani S, Vuyelwa N, Kodama T, Oluwafemi OS. Cytotoxicity evaluation of graphene oxide against adherent and suspension cancer cells. Mater Lett. 2020;279:128470.
[34] Guo H, Zhang X, Chen Z, Zhang L, Wang L, Xu J, et al. High-energy short-wave blue light conversion films via carbon quantum dots for preventing retinal photochemical damage. Carbon. 2022;199:431–8.
[35] Varsha Raveendran PT, Renuka NK. Carbon dots as a sustainable alternative to plant extracts for the green synthesis of noble metal nanoparticles. Environ Nanotechnol Monit Manag. 2022;18:100676.
[36] Guo H, et al. One-pot synthesis of orange emissive carbon quantum dots for all-type high color rendering index white light-emitting diodes. ACS Sustain Chem Eng. 2022;10(26):8289–96.
[37] Dembereldorj U, Choi SY, Ganbold EO, Song NW, Kim D, Choo J, et al. Gold nanorod-assembled PEGylated graphene-oxide nanocomposites for photothermal cancer therapy. Photochem Photobiol. 2014;90(3):659–66.
[38] Lebepe TC, Oluwafemi OS. Thermal and medium stability study of polyvidone-modified graphene oxide-coated gold nanorods with high photothermal efficiency. Nanomaterials. 2022;12(19):3382.
[39] Oladipo AO, Lebepe TC, Ncapayi V, Tsolekile N, Parani S, Songca SP, et al. The therapeutic effect of second near-infrared absorbing gold nanorods on metastatic lymph nodes via lymphatic delivery system. Pharmaceutics. 2021;13(9):1359.
[40] Wang L, et al. Ultrastable amine, sulfo cofunctionalized graphene quantum dots with high two-photon fluorescence for cellular imaging. ACS Sustain Chem Eng. 2018;6(4):4711–6.
[41] Yuan B, Sun X, Yan J, Xie Z, Chen P, Zhou S. C96H30 tailored single-layer and single-crystalline graphene quantum dots. Phys Chem Chem Phys. 2016;18(36):25002–9.
[42] Tsai M-F, Chang SH, Cheng FY, Shanmugam V, Cheng YS, Su CH, et al. Au nanorod design as light-absorber in the first and second biological near-infrared windows for in vivo photothermal therapy. ACS Nano. 2013;7(6):5330–42.
[43] Wang Y-H, Chen SP, Liao AH, Yang YC, Lee CR, Wu CH, et al. Synergistic delivery of gold nanorods using multifunctional microbubbles for enhanced plasmonic photothermal therapy. Sci Rep. 2014;4(1):5685.
[44] Liu C, Huang Y, Zhao C, Yang F, Qin H, Wang Z. Cell biophysical characteristics of PPy-GNPs and their application in photothermal therapy of SKOV-3 cell. J Nanopart Res. 2020;22(9):284.
[45] Li Y, Xu Q, Shi M, Gan P, Huang Q, Wang A, et al. Low-level laser therapy induces human umbilical vascular endothelial cell proliferation, migration and tube formation through activating the PI3K/Akt signaling pathway. Microvasc Res. 2020;129:103959.